Journal of Power Sources 191 (2009) 390–399

Contents lists available at ScienceDirect

Journal of Power Sources

journal homepage: www.elsevier.com/locate/jpowsour

Evaluation of the net water transport through electrolytes in Proton Exchange Membrane Fuel Cell

Dongryul Lee, Joongmyeon Bae*

Department of Mechanical Engineering, School of Mechanical, Aerospace & Systems Engineering, Korea Advanced Institute of Science and Technology, 373-1 Guseong-dong, Yuseong-gu, Daejeon 305-701, Republic of Korea

ARTICLE INFO

Article history:
Received 6 January 2009
Received in revised form 17 February 2009
Accepted 18 February 2009
Available online 4 March 2009

Keywords:
PEMFC (Proton Exchange Membrane Fuel Cell)
CFD analysis
Net water transport
Species mole fraction
Ionic conductivity
Activation loss

ABSTRACT

Electro-osmotic drag and back diffusion are the primary water transport mechanisms in PEMFC (Proton Exchange Membrane Fuel Cell) electrolytes. These two phenomena occur competitively in the membrane, and ultimately determine the net water movement. The chemical compositions of reactants and product (i.e., H_2, O_2, and H_2O) in a porous catalyst layer vary with respect to the electro-chemical reactions and water transport through the membrane. The tendency of the chemical compositions was estimated by analyzing the net water transport coefficient (α), defined as the ratio of the reaction rate to the water transport rate. New criteria were suggested for predicting species mole fractions from the flow direction, and these were validated by CFD analysis. The hydrogen mole fraction had different tendencies to rise or fall based on the flow direction at $\alpha = 0.5$, while the oxygen mole fraction extreme was located at $\alpha = -0.75$. Finally, α was shown to influence the membrane conductivity and activation losses, which are the main factors that contribute to fuel cell performance.

Published by Elsevier B.V.

1. Introduction

Worldwide energy consumption is sharply rising, and new environmental regulations will soon be implemented in an effort to reduce atmospheric carbon dioxide levels, which can influence global warming. Many countries are concentrating on developing clean and renewable energy systems. Fuel cells present an environmentally friendly and efficient energy conversion system that has been considered as an alternative power source. Additionally, fuel cells have a high potential for commercialization due to continuing research. PEMFCs (Proton Exchange Membrane Fuel Cell) are low-temperature fuel cells that can be used for FCVs (Fuel Cell Vehicles) or RPG (Residential Power Generation) systems. It is proposed that FCVs will be the biggest market in 10 years; thus, major automobile companies throughout the world have concentrated on commercializing PEMFCs. However, long-term stability, sub-zero operation, and competitive prices must be achieved.

To maintain stable and efficient operation of PEMFCs, irreversible losses such as activation losses, ohmic losses, and concentration losses, must be minimized. Activation losses are unavoidable when generating current from a fuel cell, and these are affected by temperature, pressure, catalyst materials, and the mole fractions of reactants. The mole fractions of reactants are related to the mass transport in a bipolar plate (BPP) channel and a gas diffusion layer (GDL). Since concentration losses originate from the process of supplying reactants and removing products, concentration losses are partially related to activation losses [1]. It is known that concentration losses account for a significant portion of the overall irreversible losses, and thus, a uniform distribution of reactant must be achieved to improve the performance of PEMFCs [2–7].

Mass transport in the cathode is more complex than in the anode, due to the complexity of oxygen diffusion and water removal. Additionally, cathode activation losses are generally larger than those in the anode because the barrier energy for the oxygen reduction reaction (ORR) is higher than for the hydrogen oxidation reaction (HOR). Therefore, a uniform oxygen distribution is important for reducing activation losses and concentration losses, and has been investigated extensively [8–16].

Humidity is also an important parameter in reducing ohmic losses because the resistance of the membrane is determined by the relative humidity. Springer et al. measured and modeled the ion conductivity of a 117 Nafion membrane with varying humidity [17]. Their results have been widely employed for estimating membrane conductivities. Buchi and Scherer compared the humidity effect at both electrodes. Two and four membranes were laid to detect the resistance of each membrane. Finally, the authors found that humidity at the anode is more influential than at the cathode when

* Corresponding author. Tel.: +82 42 350 3045; fax: +82 42 350 3210.
E-mail address: jmbae@kaist.ac.kr (J. Bae).

0378-7753/$ – see front matter. Published by Elsevier B.V.
doi:10.1016/j.jpowsour.2009.02.053

Nomenclature

a_k	water activity in stream k
A_{cv}	specific surface area of control volume (m^{-1})
$Area_{cv}$	surface area of control volume (m^2)
C_n	concentration of species n ($mol\,m^{-3}$)
$D_{n,j}$	diffusion coefficient of species n in mixture j ($m^2\,s^{-1}$)
$D'_{n,j}$	diffusion coefficient of species n in mixture j through porous media ($m^2\,s^{-1}$)
d	diffusion adjustment (%)
$D_{H_2,l}$	diffusion coefficient of H_2 in liquid-water film ($6.3e{-}9\,m^2\,s^{-1}$)
$D_{O_2,l}$	diffusion coefficient of O_2 in liquid-water film ($2.4e{-}9\,m^2\,s^{-1}$)
F	Faraday constant ($96{,}487\,C\,mol^{-1}$)
$H_{H_2,l}$	Henry's law constant for H_2 in liquid-water film (8.9e9 Pa)
$H_{O_2,l}$	Henry's law constant for O_2 in liquid-water film (2.12e10 Pa)
h_{rxn}	enthalpy for water formation ($kJ\,kmol^{-1}$)
h_{fg}	enthalpy for water vaporization ($kJ\,kg^{-1}$)
I	local current density ($A\,m^{-2}$)
$I_{0,n}$	exchange current density for n ($A\,m^{-2}$)
$m_{n,k}$	mass fraction of species n in stream k
M_n	equivalent weight of n ($kg\,mol^{-1}$)
$mass_n$	mass of species n (kg)
n_d	electro-osmotic drag coefficient
P	pressure (Pa)
P_n	partial pressure of species n (Pa)
R	universal gas constant ($8.314\,J\,mol^{-1}\,K^{-1}$)
r	condensation rate ($m^{-3}\,s^{-1}$)
S	source terms
S_{he}	heat source term from electrochemical losses
S_{hp}	heat source term from water phase change
t_m	membrane thickness (m)
$t_{f,k}$	liquid-water film on the k (anode or cathode) (m)
T	temperature (K)
u	velocity ($m\,s^{-1}$)
V_{oc}	open-circuit voltage (V)
V_{cell}	cell voltage (V)
$X_{n,k}$	mole fraction of species n in stream k
$[n]$	molar flux of species n ($mol\,s^{-1}\,m^{-2}$)
k	thermal conductivity ($W\,m^{-1}\,K^{-1}$)

Greek symbols

ε	porosity
η	kinetic overpotential (V)
μ	dynamic viscosity ($kg\,s^{-1}\,m^{-1}$)
ρ	density ($kg\,m^{-3}$)
α	net water flux per proton flux through membrane
α_k	kinetic transfer coefficient for reaction k
σ_m	membrane conductivity ($S\,m^{-1}$)
β	permeability (m)

Superscript

sat	saturation

Subscript

a	anode
c	cathode
e	electrochemical reaction
p	phase change
H_2	hydrogen
O_2	oxygen
l	liquid
v	water vapor
H_2O	water
ξ	dummy variable for direction x, y, or z
rxn	reaction
oxi	oxidation at anode by reaction
red	reduction at cathode by reaction
drag	electro-osmotic drag through membrane from anode to cathode
back	back diffusion through membrane from cathode to anode
gen	water generation at the cathode by reaction
van	vanished water at cathode

the membrane thickness is less than 50 μm [18]. In other words, hydrogen has to be well humidified to minimize ohmic losses.

As discussed, a uniform oxygen distribution at the cathode and high relative humidity at the anode are necessary conditions to improve the performance of PEMFCs. These two conditions can be satisfied without external humidification when the membrane is self-humidified by water generated from fuel-cell reactions. Back diffusion can decrease activation losses and increase membrane conductivity. Vengatesan et al. suggested that the performance of PEMFCs can be enhanced by using a thin cast membrane [19]. In this setup, the membrane conductivity can be properly maintained by the back diffusion. The possibility of internal humidification was also mentioned by Buchi and Srinivasan [20]. It was also reported that back diffusion is intensified by adding hydrophilic SiO_2 particles to the catalyst layers at anode, and cell performance is improved at low relative humidity [21]. However, the relationship between water movement through the membrane and cell performance has not been clearly defined in the literatures.

The net water movement through the membrane and the fuel-cell reactions are linked to each other and can cause the chemical composition to vary. For example, the composition of the anode stream is determined by the water transport from electro-osmotic drag and the HOR. In contrast, species mole fractions in the cathode can be estimated from the water back-diffusion rate and the water-generation rate (or alternatively, the oxygen reaction rate). Consequently, in this study, each species mole fraction in the anode and/or the cathode and the net water movement are shown to be related and have the influence for the membrane conductivity and activation losses. Criteria are suggested for predicting the rise and fall in the oxygen mole fraction, the water mole fraction in the anode, and the irreversible losses. CFD analysis was used to validate the relationship between the mole fraction change of each species in the catalyst layer and the net water flux through the membrane.

2. Mathematical formulation

Mass, momentum, and energy conservation equations were used as the governing equations for simulating a PEMFC. Species transport equations for hydrogen, oxygen, and water were also used to predict the changes in mole fractions in the anode and cathode. The following assumptions were applied in the PEMFC model: steady state, laminar flow in the channel, high electronic conductivity in the bipolar plate (BPP) for uniform galvanic potential, and homogeneous two-phase flow [8].

The mass conservation equations are as follows:

$$\nabla \cdot (\rho \vec{u}) = S_m \tag{1}$$

$$S_m = S_{H_2} + S_{wvp} + S_{wlp} + S_{awve} \quad \text{at } z = z_3 \tag{1.1}$$

$$S_m = S_{O_2} + S_{wvp} + S_{wlp} + S_{cwve} \quad \text{at } z = z_2 \tag{1.2}$$

where,

$$S_{H_2} = -\frac{I(x,y)}{2F} M_{H_2} A_{cv} \quad \text{at } z = z_3 \tag{2.1}$$

$$S_{O_2} = -\frac{I(x,y)}{4F} M_{O_2} A_{cv} \quad \text{at } z = z_2 \tag{2.2}$$

$$S_{awv_e} = -\frac{\alpha(x,y)}{F} I(x,y) M_{H_2O} A_{cv} \quad \text{at } z = z_3 \tag{2.3}$$

$$S_{cwv_e} = \frac{1 + 2\alpha(x,y)}{2F} I(x,y) M_{H_2O} A_{cv} \quad \text{at } z = z_2 \tag{2.4}$$

$$S_{wlp} = -S_{wvp} = -\frac{M_{H_2O} \sum_{n\,of\,v} (\text{mass}_{n\,of\,v}/M_{n\,of\,v})}{(1 - (P_{wv}^{sat}/P))} \left(\frac{P_{wv}^{sat} - P_{wv}}{P} \right) r \tag{2.5}$$

The mass change of each species due to reaction is described by Eqs. (2.1)–(2.4). The phase change between water vapor and liquid water is affected by the saturation pressure and defined by Eq. (2.5), where r is the condensation rate ($1\ m^{-3}\ s^{-1}$). The liquid water can move to the vapor phase by evaporation if the partial pressure of liquid water is higher than the saturation pressure.

The momentum conservation equations are as follows:

$$\nabla \cdot (\rho \vec{u} \vec{u}) = -\nabla P + \nabla \cdot (\mu \nabla \vec{u}) + S_p, \tag{3}$$

where,

$$S_p = -\frac{\mu}{\beta} \vec{u} \quad \text{at } z_2 \le z \le z_{1'} \text{ and } z_1 \le z \le z_3 \tag{3.1}$$

The momentum sink terms, defined by Eq. (3.1), originate from Darcy's law and are used for modeling the pressure drop in the porous catalyst layer. The permeability (β) is very small ($1.0e{-}12\ m^2$) and assumed to be isotropic. Therefore, the source terms are derived from the Navier–Stokes equation because the other terms become negligible [5].

The energy conservation equations are as follows:

$$\nabla(\rho \vec{u} h) = \nabla \cdot (k \nabla T) + S_{hp} + S_{he} \tag{4}$$

where,

$$S_{he} = h_{rxn} \times \left(\frac{I(x,y) \times A_{cv}}{2F} \right)_{z=z_2} - (I(x,y) \times V_{cell} \times A_{cv})_{z=z_2} \quad \text{at } z = 0 \tag{4.1}$$

$$S_{hp} = S_{wlp} \times h_{fg}. \tag{4.2}$$

The difference between the total chemical energy of the reactants and the electrical work was assumed to be released as heat. Since h_{rxn} is for the overall chemical reaction between H_2 and O_2, the heat of reaction is assumed to be generated at the middle of the membrane, and not on the catalyst surface. Latent heat due to phase change is also contained in the heat source terms and is evaluated by the enthalpy of formation of water, h_{fg}. The flow and thermal properties in the GDL, the BPP, and the membrane are shown in Table 1.

The species transport equations are as follows:

$$\nabla \cdot (\rho m_n \vec{u}) = \nabla \cdot (J_n) + S_n, \tag{5}$$

where n denotes the species, H_2, O_2, water vapor, or liquid water. The change in the mass fraction resulting in electrochemical reactions is reflected by the source terms in the species equations. These source terms are the same as for the mass conservation equations.

Table 1
Flow and thermal parameter in the GDL, the BPP, and the membrane [23].

Porosity in the GDL	0.7
Permeability in the GDL	$1.0e{-}12\ m$
Diffusion adjustment	50%
GDL thermal conductivity	$0.21\ W\ m^{-1}\ K^{-1}$
BPP thermal conductivity	$5.7\ W\ m^{-1}\ K^{-1}$
Membrane thermal conductivity	$0.15\ W\ m^{-1}\ K^{-1}$

The equations and parameters used to model the electrochemical phenomena are shown in Tables 2 and 3. The water activity indicates the humidity at the membrane (Eq. (8)), and the water content (λ) represents the number of water molecules per sulfuric acid bonds in the membrane (Eq. (9)). The membrane conductivity was determined by the water activity and water content (Eq. (14)). It is known that ohmic losses are more significantly affected by the humidity at the anode than at the cathode when the membrane is less than 50 μm [18]. Therefore, the membrane conductivity (σ_m) can be evaluated from the water content, based on the anode water activity.

Two main water transport phenomena occur in the electrolyte of PEMFCs. Electro-osmotic drag (n_d) results from proton movements that promote water transport from the anode to the cathode (Eq. (10)). Back diffusion is caused by a concentration difference that promotes water diffusion from the cathode to the anode, and was modeled by the water diffusivity of the membrane (Eq. (11)) and the water concentration (Eq. (12)). The net water flux per proton through the membrane (α) is defined by the flux difference of electro-osmotic drag and back diffusion (Eq. (13)). By definition, water is transported from the anode to the cathode if α is positive, and vice versa. All of the source terms in Eq. (2.1)–(2.5) are linked because α is included in each.

The activation loss (η) was estimated by the Tafel equation, as shown in Eq. (15) [1]. The exchange current density (I_0) is modified by the hydrogen or oxygen mole fraction in the natural logarithm of Tafel equation. The concentration loss can be included in the activation loss by modifying the exchange current density. The cathode activation loss (η_c) is generally higher than in the anode due to the complexity of the ORR. Therefore, the total activation loss is determined dominantly by the cathode activation loss and the oxygen mole fraction.

Current densities were calculated from Eq. (16), considering the open-circuit voltage (OCV) and irreversible losses. The local membrane conductivity and activation losses are the main influencing factors for the current densities.

Liquid water is formed when the water partial pressure is higher than the saturation pressure. It is assumed that the catalyst layer is partially covered by a thin liquid film [23]. Hydrogen and oxygen dissolve in the film according to Henry's law (Eq. (17)). The diffusion length of soluble gas is determined by the thickness of the liquid-water film. The thickness of liquid water is modeled by Eq. (18), as discussed in the appendix of Lee et al. [16].

All governing equations and appropriate boundary conditions were solved using the commercial CFD tool STAR CD ver. 3.26, with custom user subroutines.

3. New criteria for prediction of the species mole fractions

The species mole fractions can be estimated in a porous catalyst layer by considering the reaction rate and the water transport through the membrane. That is, the variation of species mole fractions can be predicted by the net water flux per proton (α) because the number of protons related to the reaction rate and net water movements through membrane are contained in α.

Table 2
Equations for the electrochemical reactions.

Variables	Equations	
Diffusion mass flux	$J_{\zeta,n} = -\rho D_{\zeta,n} \frac{\partial m_{K,n}}{\partial \zeta}$	(6)
Binary diffusion coefficient [22,23]	$\frac{PD_{n,j}(x,y)}{(P_{c,n} \times P_{c,j})^{1/3}(T_{c,n} \times T_{c,j})^{5/12}(1/M_n + 1/M_j)^{1/2}} = 3.64 \times 10^{-8} \left(\frac{T(x,y)}{\sqrt{T_{c,n}T_{c,j}}} \right)^{2.334}$	(7)
	$D'_{n,j}(x,y) = d \times D_{n,j}(x,y)$ in porous media	
Water activity	$a_K = \frac{X_{w,K}P(x,y)}{P^{sat}_{w,K}}$	(8)
Water content in the membrane [17]	$\lambda = 0.043 + 17.81a_a - 39.85a_a^2 + 36a_a^3 \quad (0 \le a_a \le 1)$ $\lambda = 14 + 1.4(a_a - 1) \quad (1 \le a_a \le 3)$	(9)
Electro-osmotic drag coefficient [11]	$n_d = 0.0029\lambda^2 + 0.05\lambda - 3.4 \times 10^{-19}$	(10)
Water diffusion coefficient in the membrane [17]	$D_W = D_\lambda \times \exp\left(2416\left(\frac{1}{303} - \frac{1}{T(x,y)}\right)\right)$	(11)
	$D_\lambda = \begin{cases} 10^{-10}, & \lambda \le 2 \\ 10^{-10}(1 + 2(\lambda - 2)), & 2 \le \lambda \le 3 \\ 10^{-10}(3 - 1.67(\lambda - 3)), & 3 \le \lambda \le 4.5 \\ 1.25 \times 10^{-10}, & 4.5 \le \lambda \end{cases}$	
Water concentration on the surfaces of the MEA [1]	$C_{w,K}(x,y) = \frac{\rho_{m,dry}}{M_{m,dry}} \times \lambda_{a\,or\,c}$	(12)
Net water flux per proton [23]	$\alpha(x,y) = n_d(x,y) - \frac{F}{I(x,y)} D_W(x,y) \frac{C_{wlc}(x,y) - C_{wla}(x,y)}{t_m}$	(13)
Local membrane conductivity [13]	$\sigma_m(x,y) = (0.514\lambda - 0.326) \times \exp\left(1268\left(\frac{1}{303} - \frac{1}{T(x,y)}\right)\right)$	(14)
Local overpotential [11]	$\eta(x,y) = \eta_c(x,y) + \eta_a(x,y) = \frac{RT_{z_2}}{\alpha_c F} \ln\left(\frac{I(x,y)}{I_{0,O_2}X_{O_2,z_2}}\right) + \frac{RT_{z_3}}{\alpha_a F} \ln\left(\frac{I(x,y)}{I_{0,H_2}X_{H_2,z_3}}\right)$	(15)
Local current density [11]	$I(x,y) = \frac{\sigma_m(x,y)}{t_m}(V_{OC} - V_{CELL} - \eta(x,y))$	(16)
Gas solubility in the liquid-water film [8]	$-\frac{I(x,y)}{2F} M_{H_2} = \rho_{H_2} D_{H_2,l} \left(\frac{X_{H_2,z_{glif,a}} P_{z_{glif,a}}/H_{H_2,l} - X_{H_2,z_3}}{t_{f,a}} \right)$ $-\frac{I(x,y)}{4F} M_{O_2} = \rho_{O_2} D_{O_2,l} \left(\frac{X_{O_2,z_{glif,c}} P_{z_{glif,c}}/H_{O_2,l} - X_{O_2,z_2}}{t_{f,c}} \right)$	(17)
Water film thickness [8]	$t_{f,k} = \frac{m_{w,l}\left(\sum \text{mass}_n\right)}{\varepsilon \rho_{wl} \text{Area}_{cv}}$	(18)

Six variables were used to compare the conversion rate of each species (Fig. 1). Hydrogen is oxidized and two protons are generated at the anode catalyst layer. Oxygen is reduced with protons which are dragged from the anode, and converted into water molecules at the cathode catalyst layer. $[H_2]_{oxi}$ is the oxidation rate of hydrogen, and $[O_2]_{red}$ is the reduction rates of oxygen. Water is dragged from the anode to the cathode ($[H_2O]_{drag}$), or in the opposite direction ($[H_2O]_{back} = -[H_2O]_{drag}$). $[H_2O]_{gen}$ is the water-generation rate at the cathode, and $[H^+]_{drag}$ is the electro-osmotic drag rate of protons through the membrane from the anode to the cathode.

Kinetic equations were derived (Eqs. (19.1) and (20.1)) from the electrochemical reactions at the anode (19) and the cathode (20). α was also derived (Eqs. (19.2) and (20.2)) at both catalyst layers from the drag rate of protons and the water transport rates.

$$H_2 \leftrightarrow 2H^+ + 2e^- \quad \text{at anode catalyst layer} \tag{19}$$

$$[H_2]_{oxi} = \frac{[H^+]_{drag}}{2} \tag{19.1}$$

$$\alpha = \frac{[H_2O]_{drag}}{[H^+]_{drag}} \tag{19.2}$$

$$2H^+ + 2e^- + \tfrac{1}{2}O_2 \leftrightarrow H_2O \quad \text{at cathode catalyst layer} \tag{20}$$

$$\frac{[H^+]_{drag}}{4} = [O_2]_{red} = \frac{[H_2O]_{gen}}{2} \tag{20.1}$$

$$\alpha = -\frac{[H_2O]_{back}}{[H^+]_{drag}} \tag{20.2}$$

New criteria for predicting the species mole fractions are suggested by Eqs. (21) and (22). These formulations are derived from the combination of kinetic equations and the definition of α. These criteria will be referred to as the 'alpha criteria' throughout this paper. If $\alpha \ge 0.5$, $[H_2O]_{drag}$ is greater than $[H_2]_{oxi}$ at the anode catalyst layer in Eq. (21), and vice versa. If $-0.5 \le \alpha \le 0$, $[H_2O]_{gen}$ is greater than $[H_2O]_{back}$ at the cathode catalyst layer in Eq. (22).

Table 3
Parameters for the electrochemical reaction [23].

Dry membrane density ($\rho_{m,dry}$)	2 kg m^{-3}
Equivalent weight of dry membrane ($M_{m,dry}$)	1.1 kg mol^{-1}
Exchange current density for hydrogen (I_{0,H_2})	0.2 A cm^{-2}
Exchange current density for oxygen (I_{0,O_2})	0.02 A cm^{-2}
Anode transfer coefficient (α_a)	1.2
Cathode transfer coefficient (α_c)	0.6

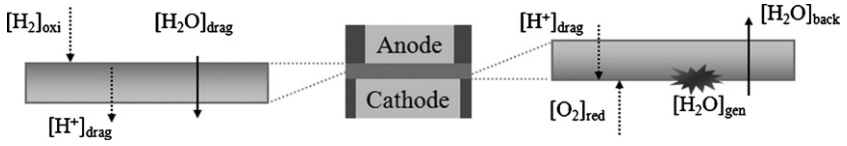

Fig. 1. Conceptual diagram of the electrochemical reaction within the catalyst layer and water movement through the membrane.

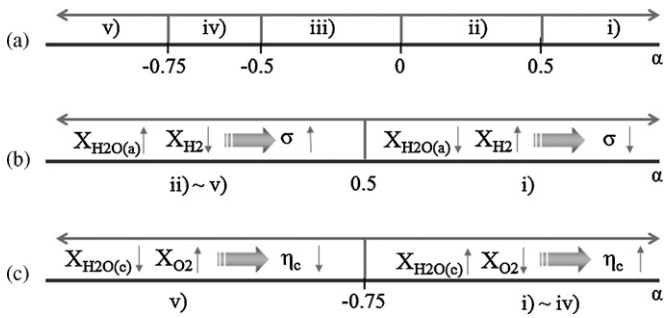

Fig. 2. Schematic diagram of the alpha criteria: five regions of α (a), mole fraction changes at the anode (b), and mole fraction changes at the cathode (c).

$[H_2O]_{van}$, defined by the difference between $[H_2O]_{gen}$ and $[H_2O]_{back}$, is smaller than $[O_2]_{red}$ when $\alpha \leq -0.75$. The direction of water movement through the membrane is determined at $\alpha = 0$ by definition. Therefore, α can be separated into five distinct regions by these four points ($\alpha = 0.5$, 0, -0.5, -0.75) to provide comparative rates at each electrode.

$$[H_2O]_{drag} = (2\alpha)[H_2]_{oxi} \quad (21)$$

$$[H_2O]_{van} = [H_2O]_{back} - [H_2O]_{gen} = -2(2\alpha + 1)[O_2]_{red} \quad (22)$$

A schematic diagram of the alpha criteria is shown in Fig. 2. The five distinct regions, regions (i)–(v), are shown in Fig. 2(a). The change in species mole fractions in the anode stream is represented in Fig. 2(b). The tendency of species composition in the anode stream can be characterized at $\alpha = 0.5$ since $[H_2O]_{van}$ is comparable to $[H_2]_{oxi}$ at $\alpha = 0.5$ from Eq. (21). In the region where $\alpha > 0.5$, the water mole fraction may decrease, or the hydrogen mole fraction may increase through the anode stream because $[H_2]_{oxi} < [H_2O]_{drag}$. If $\alpha \leq 0.5$, the anode water mole fraction may increase, or the hydrogen mole fraction may decrease. The rise and fall of the membrane conductivity will be influenced by these tendencies of the water mole fraction in anode. The change in species mole fractions in the cathode stream is represented in Fig. 2(c). The tendency of species composition in the cathode stream can be characterized at $\alpha = -0.75$ since $[H_2O]_{drag}$ is comparable to $[O_2]_{red}$ at $\alpha = -0.75$ from Eq. (22). The water mole fraction may increase or the oxygen mole fraction may decrease through the cathode stream in the region where $\alpha > -0.75$ because $[H_2O]_{van} < [O_2]_{red}$. If $\alpha \leq -0.75$, the cathode water mole fraction may decrease, or the oxygen mole fraction may increase. The rise and fall of activation losses will be influenced by these tendencies of oxygen mole fraction in the cathode. In summary, changes in the behavior of each species along the flow direction are dissimilar before and after $\alpha = 0.5$ for the anode, and before and after $\alpha = -0.75$ for the cathode. These tendencies can be linked to membrane conductivity, anode and cathode activation losses, and current density. Among these parameters, membrane conductivity and the cathode activation losses will be investigated using the alpha criteria.

Table 4
Boundary conditions.

Inlet flow temperature	70 °C
Inlet humidity (case number)	Anode: 100% Cathode: 70% (1), 80% (2), 90% (3)
Inlet humidity (case number)	Anode: 70% (4), 75% (5), 80% (6) Cathode: 100%
Stoichiometry	6 (anode and cathode)
Temperature at BPP surface	70 °C

4. Computational domain

4.1. Grids without gas diffusion layers (GDLs)

The computational domain for validating the alpha criteria is shown in Fig. 3. The mid-plane of the membrane is located at $z = 0$. The membrane thickness is 50 μm, which is the distance between Z_1 and $Z_{1'}$. The thicknesses of the catalyst layer and the channel are 100 and 250 μm, respectively. The interfaces between the channel and the porous catalyst layer are at Z_2 and Z_3. The flow channel is approximately 2 cm long in the x direction. A total of 20,800 nodes were used to model the PEMFC ($120 \times 8 \times 5$ nodes for both the anode and the cathode channels and $100 \times 8 \times 4$ nodes (membrane), 3 nodes (both BPPs), or 2 nodes (both catalyst layers)).

To accurately predict the behavior of the species mole fractions using our new criteria, gas diffusion layers are not introduced in Fig. 3. When the gas diffusion layers are included, concentration gradients appear at the porous medium. It was found that this results in an error in the estimation of the alpha criteria. Additionally, the ribs of the interconnector are not included in the computational domain to consider the one-dimensional changes of species mole fractions in the x direction. The stoichiometry at both the anode and the cathode channels was set at 6. High stoichiometries and the small volume of the porous medium (from neglecting the GDLs) made the species concentration uniform in the z direction. These limitations will be addressed in Section 5 with an analysis of the results including the GDLs and the ribs under realistic stoichiometric conditions.

Hydrogen and water, provided by a humidifier, were injected in the anode channel. Oxygen, instead of air, and steam were injected in the cathode channel. The humidity conditions were controlled to determine the net water movement through the membrane. Six cases were applied to the grids without GDLs to verify the alpha criteria (Table 4). Electro-osmotic drag will be more active than back diffusion in cases 1–3 due to the high relative humidity at the anode. However, water will move from the cathode to the anode by back

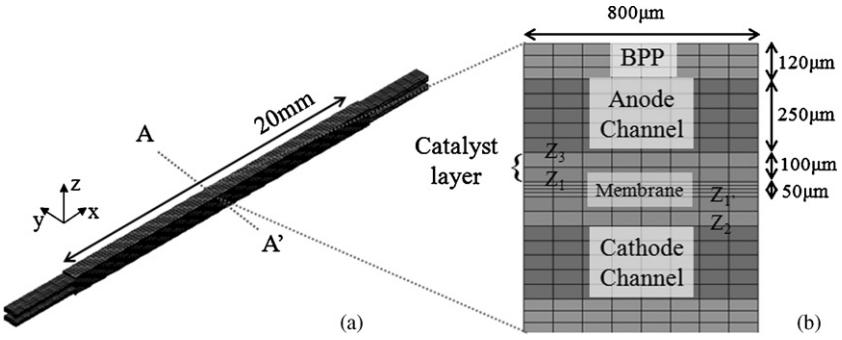

Fig. 3. Computational domain of a single straight channel flow field for a PEMFC without GDLs: (a) geometry and (b) cross-sectional view.

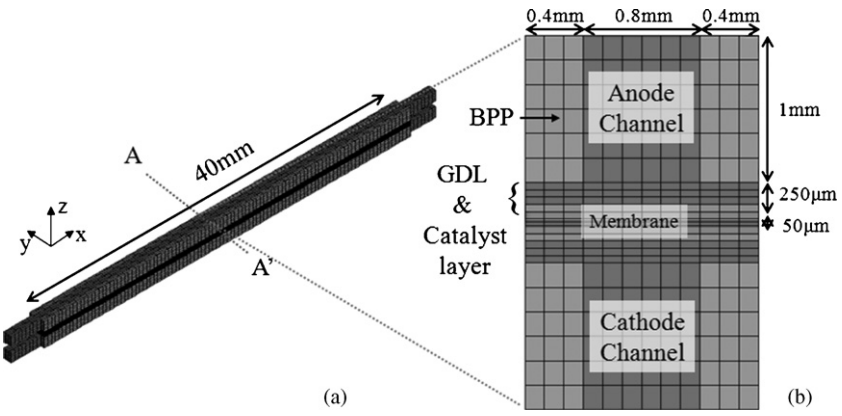

Fig. 4. Computational domain of a single straight channel flow field for a PEMFC with GDLs: (a) geometry and (b) cross-sectional view.

diffusion in cases 4–6 because of the high relative humidity at the cathode. The flow directions in the anode and cathode were the same in the positive x direction. The current density was 0.3 A cm^{-2} for all cases. Results were extracted from the lines located at $y = 0$ and $z = Z_1$ or $Z_{1'}$.

4.2. Grids for a real PEMFC with GDLs

Negligible vertical flow between the porous catalyst layer and the channel and one-dimensional concentration change were assumed, in order to limit the computational domain. However, in real PEMFCs, the channel thickness is usually greater than 1 mm, and the GDL is located between the channel and the catalyst layer. Therefore, reactant and product concentrations are non-uniform throughout the diffusion medium. Additionally, species concentration changes are no longer one-dimensional if the ribs are included in the computational domain.

A new PEMFC grid with GDLs and ribs was made for comparison with Fig. 3. The grid and dimensions, which has 32,352 nodes, are shown in Fig. 4. The channel length was 4 cm. The humidity conditions were the same as case 1 of Table 4. More realistic stoichiometries were used, 1.2 in the anode and 2.0 in the cathode. Humidified hydrogen and air were injected in the anode and cathode channel. The current density was 0.6 A cm^{-2} and the results were extracted from the center line in the x direction at the catalyst layer.

5. Results and discussion

5.1. Net water flux per proton (α)

The net water transfer coefficient per proton is shown in Fig. 5. Water moved from the anode to the cathode at the inlet region, as shown in Fig. 5(a), due to the fully saturated humidity condition at anode. Water diffused from the cathode to the anode at the outlet region. Back diffusion was very active over the entire area in cases 4–6 (Fig. 5(b)). Dashed lines are drawn at $\alpha = 0.5$ and -0.75, where the water mole fraction at the anode and the oxygen mole fraction at the cathode show different tendencies because of the alpha criteria. The locations of $\alpha = 0.5$ were at $x/L = 0.28$ for case 1, 0.23 for case 2, and 0.155 for case 3, and the points in which $\alpha = -0.75$ were represented at $x/L = 0.29$ for case 4, 0.235 for case 5, and 0.14 for case 6.

5.2. Water mole fraction at the anode and the membrane conductivity

The water mole fraction at the anode is shown in Fig. 6. There is a decreasing area of water mole fraction in Fig. 6(a) because water is removed relatively faster than hydrogen in region (i). The water mole fraction at the anode increased, except in region (i), as previously predicted by the alpha criteria. The increasing tendency of the anode water mole fraction along the flow direction was maintained in the outlet region in Fig. 6(a) and over the entire area in Fig. 6(b). This is because the HOR rate is higher than the water transport rate, or water is accumulated by back diffusion.

The membrane conductivity showed the same tendency as the water mole fraction at the anode. The conductivity in the inlet region decreased due to the drop in the anode water mole fraction, in Fig. 7(a). However, the membrane conductivity increased

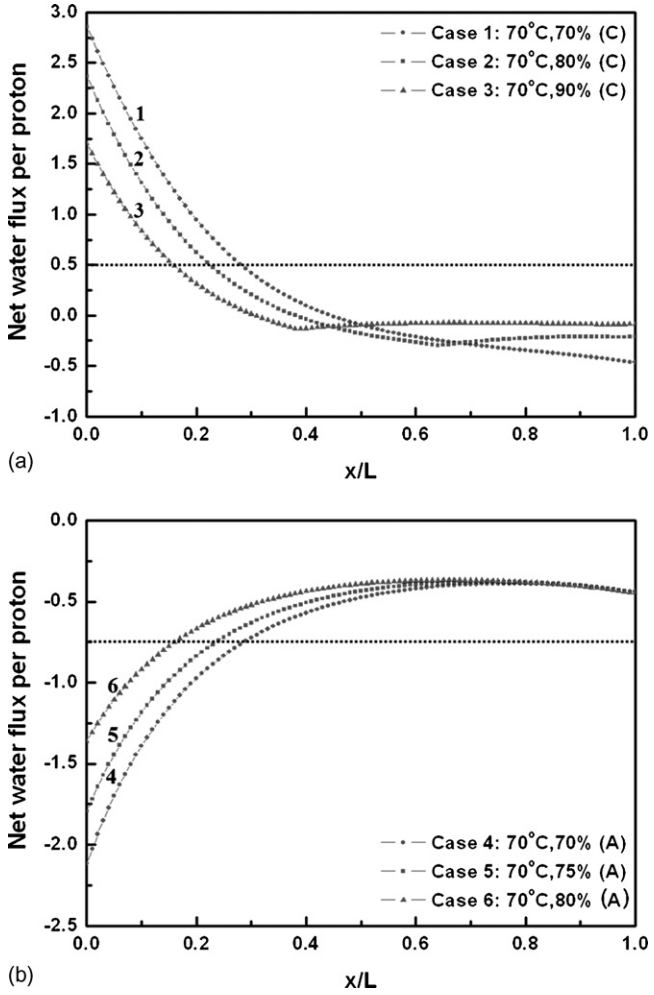

Fig. 5. Net water flux per proton along the x axis at the catalyst layers: cases 1–3 (a) and cases 4–6 (b).

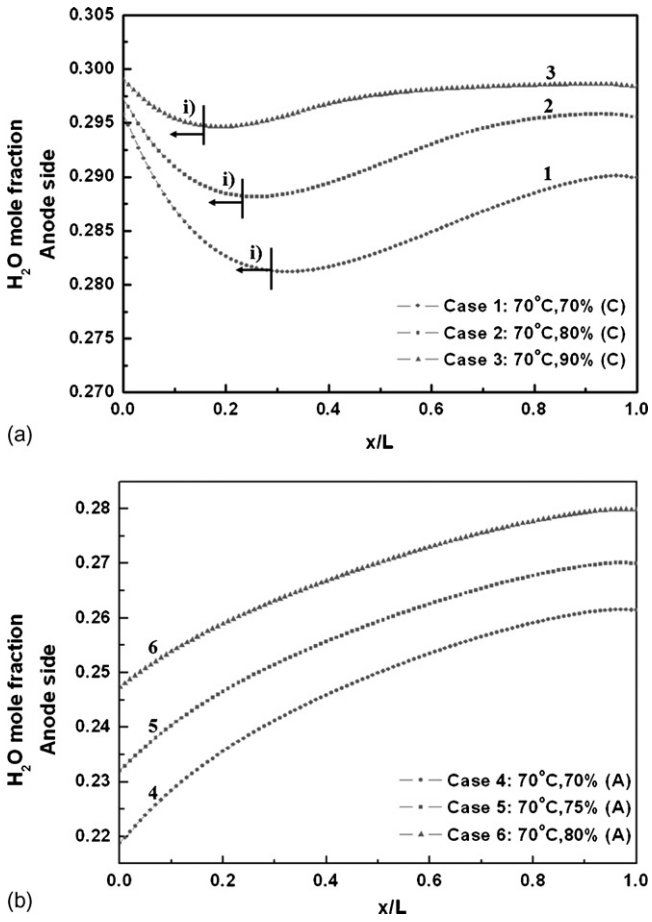

Fig. 6. Water mole fraction along the *x* axis at the anode catalyst layers: cases 1–3 (a) and cases 4–6 (b).

in the outlet region in Fig. 7(a) and over the entire area in Fig. 7(b).

5.3. Oxygen mole fraction and cathode activation losses

The oxygen mole fraction at the cathode is shown in Fig. 8. The oxygen mole fraction decreased in Fig. 8(a) and (b), except in region (v). In these cases, the rate of water accumulation from electro-osmotic drag or back diffusion was lower than the ORR rate. In contrast, the oxygen mole fraction increased in region (v), where strong back diffusion occurred (Fig. 8(b)).

The tendency of the oxygen mole fraction has an influence on the cathode activation losses. Cathode activation losses increased, as shown in Fig. 9(a) and (b), except in region (v). This was due to the diminution of the oxygen mole fraction. However, the cathode activation loss increased in region (v) (Fig. 9(b)) as opposed to being reduced due to the rise in the oxygen mole fraction.

From Eq. (15), it is observed that the current density and the oxygen mole fraction are the main factors influencing the activation losses. The activation loss will increase due to the increase in current density or the decrease in the oxygen mole fraction. In cases 1–3, the current density weakened along the flow direction (Fig. 10(a)). The tendencies of current density were expected to cause the cathode activation losses to decrease; however, the cathode activation losses increased in Fig. 9(a). Therefore, it can be concluded that the oxygen mole fraction played a dominant role in cases 1–3. In contrast, the current density increased along the flow direction in cases 4–6 (Fig. 10(b)), and cathode activation losses increased in region (v), in Fig. 8(b). Therefore, current density proved to be more influential in cathode activation losses than the oxygen mole fraction in the inlet region, shown in Fig. 8(b). It can be deduced that the cathode activation losses must be evaluated with respect to both oxygen mole fraction and current density.

5.4. General rules for the 'alpha criteria'

It was observed that the species mole fractions in the catalyst layer are influenced by the net water transfer coefficient per proton. General rules for the 'alpha criteria' can be summarized as follow:

Region (i) ($0.5 \leq \alpha$):
Anode: $0 < [H_2]_{oxi} < [H_2O]_{drag}$
Cathode: $[H_2O]_{van} = [H_2O]_{back} - [H_2O]_{gen} < 0 < [O_2]_{red}$

The water transport rate from the anode to the cathode is higher than the HOR rate at the anode catalyst layer. It seems that water is removed relatively faster than hydrogen in the anode stream of the BPP channel or the GDLs. Therefore, the hydrogen mole fraction increases and the water mole fraction decreases at the anode along the flow direction in this region. The membrane conductivity may weaken due to this tendency of the anode water mole fraction.

In the cathode, water is significantly accumulated with generation and movement from the anode. Therefore, as the water mole fraction increases, the oxygen mole fraction decreases in this region. The decrease in the oxygen mole fraction affects the increase in the

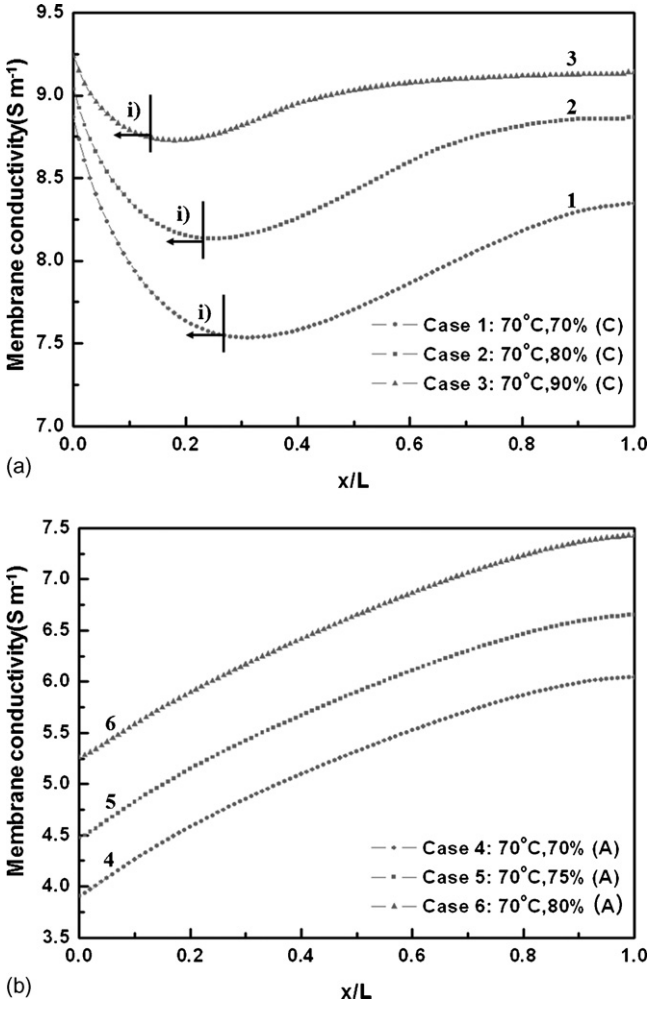

Fig. 7. Membrane conductivity along the *x* axis: cases 1–3 (a) and cases 4–6 (b).

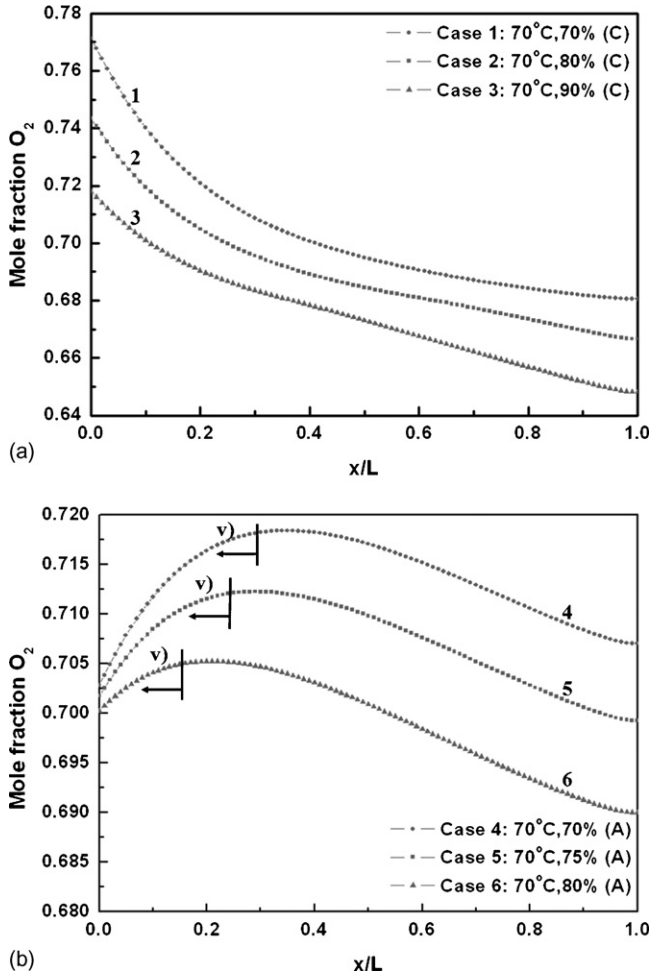

Fig. 8. Oxygen mole fraction along the x axis at the cathode catalyst layers: cases 1–3 (a) and cases 4–6 (b).

cathode activation losses. Finally, the total activation losses may increase in this region.

Region (ii) ($0 \le \alpha \le 0.5$):
Anode: $0 < [H_2O]_{drag} < [H_2]_{oxi}$
Cathode: $[H_2O]_{van} = [H_2O]_{back} - [H_2O]_{gen} < 0 < [O_2]_{red}$

The reaction rate of hydrogen is higher than the water transport rate from the anode to the cathode. Therefore, hydrogen is removed relatively faster than water in the anode stream. The hydrogen mole fraction decreases and the water mole fraction at the anode increases along the flow direction in this region. The membrane conductivity may be enhanced due to the increase in the water mole fraction in the anode.

In the cathode, water is also accumulated with generation and movement from the anode since water is transported from the anode to the cathode. Therefore, the tendencies of the oxygen mole fraction and the water mole fraction are similar to those in region (i). The oxygen mole fraction decreases and the water mole fraction increases. The decrease in the oxygen mole fraction affects the increase in the cathode activation losses. Thus, the total activation losses may also increase in this region.

Region (iii)–(v) at the anode ($\alpha \le 0$):
Anode: $[H_2O]_{drag} < 0 < [H_2]_{oxi}$

When α is negative, water is transported from the cathode to the anode. Therefore, water is accumulated by back diffusion at the anode. Hydrogen is oxidized and removed at the catalyst surface, but water is accumulated in the anode stream. Therefore, the tendency of the water and hydrogen mole fractions for negative α is similar to those in region (ii), at the anode. The hydrogen mole fraction decreases, and the water mole fraction at the anode increases along the flow direction. The membrane conductivity may increase due to the behavior of the water mole fraction at the anode when $\alpha \le 0$.

Region (iii) at the cathode ($-0.5 \le \alpha \le 0$):
Cathode: $[H_2O]_{van} = [H_2O]_{back} - [H_2O]_{gen} < 0 < [O_2]_{red}$

In region (iii), the water-generation rate is greater than the back-diffusion rate at the cathode. Water is accumulated at the cathode for this reason, although water movement through the membrane occurs from the cathode to the anode. The oxygen mole fraction decreases along the flow direction at the cathode because the oxygen is reduced at the catalyst. Thus, the total activation loss may increase in region (iii).

Region (iv) at the cathode ($-0.75 \le \alpha \le -0.5$):
Cathode: $0 < [H_2O]_{van} = [H_2O]_{back} - [H_2O]_{gen} < [O_2]_{red}$

In this region, the back-diffusion rate is greater than the water-generation rate. That is, water is removed at the cathode catalyst layer by back diffusion even though water is generated from the ORR. However, oxygen is more quickly reduced than water is removed. For this reason, the oxygen mole fraction decreases, and the water mole fraction increases along the flow direction at the

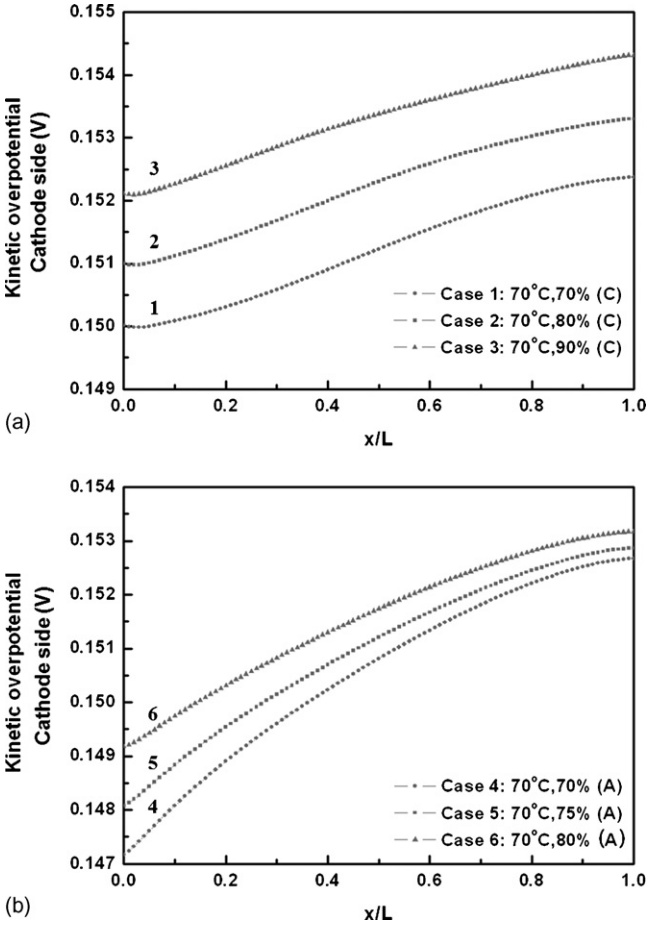

Fig. 9. Cathode activation losses along the x axis: cases 1–3 (a) and cases 4–6 (b).

cathode. With the change in the oxygen mole fraction, the total activation losses may still increase in region (iv).

Region (v) at the cathode ($\alpha \leq -0.75$):
Cathode: $0 < [O_2]_{red} < [H_2O]_{van} = [H_2O]_{back} - [H_2O]_{gen}$

Back diffusion is so strong in this region that water is more quickly removed at the cathode catalyst layer than oxygen. The oxygen mole fraction increases in this region while the water mole fraction decreases along the flow direction. These tendencies may affect the diminution of the total activation loss.

5.5. The relationship between water movement through the membrane and species mole fraction in a real PEMFC with GDLs and BPP ribs at low stoichiometric conditions

The results shown in Figs. 5–10 describe the situation for PEMFCs operating without GDL at high stoichiometry. However, GDLs are generally sandwiched between the channel and the porous catalyst layer, and the stoichiometry is not greater than 4 in a real PEMFC. Therefore, the relationship between water movement through the membrane and the species mole fractions at the catalyst layer should be analyzed at realistic PEMFC operating conditions. To revaluate the alpha criteria for these conditions, a new grid was used, as shown in Fig. 4. As previously mentioned in Section 4.2, the relative humidity at the inlet was the same as case 1, and the current density was 0.6 A cm^{-2}. The stoichiometries were set at 1.2 in the anode and 2.0 in the cathode.

The net water transfer flux per proton (α) is shown in Fig. 11(a). The point $\alpha = 0.5$ was located at $x/L = 0.07$ in the PEMFC with GDLs and ribs. The maximum hydrogen mole fraction was at $x/L = 0.15$, as shown in Fig. 11(b). Some errors occurred in predicting the maximum hydrogen mole fraction from the alpha criteria. As GDLs were added in a new computational domain at low stoichiometry, the concentration gradient through the diffusion layer became influential for the species composition in the catalyst layer. The species mole fractions in the catalyst layer were not determined only by proton and water movement through the membrane, but also by the diffusion rate of hydrogen and oxygen from the GDL. For this reason, it is difficult to accurately estimate the tendency of species mole fractions at the catalyst layer by considering only alpha criteria, as shown in Fig. 11(b).

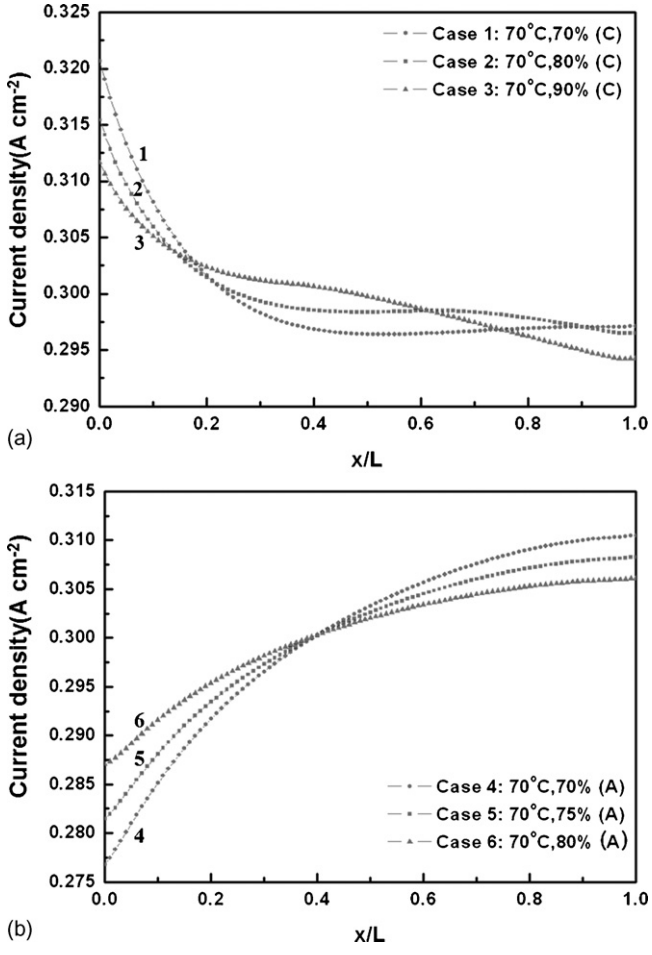

Fig. 10. Current density along the x axis: cases 1–3 (a) and cases 4–6 (b).

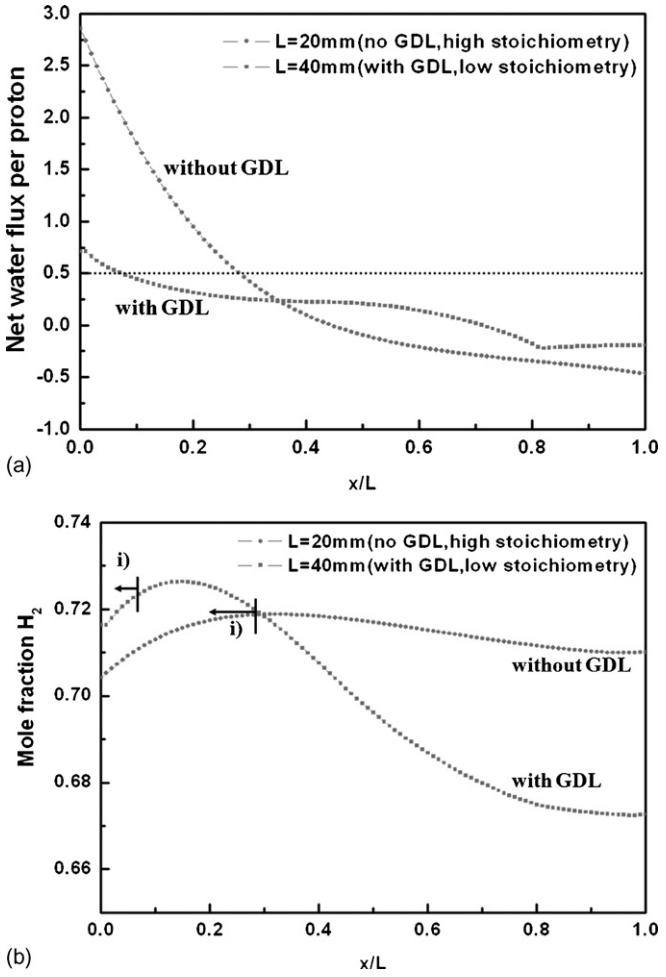

Fig. 11. Comparison between case 1 and the new case with GDL and low stoichiometry: net water transfer coefficient per proton (α) (a) and hydrogen mole fraction in the anode catalyst layer (b).

Although the alpha criteria are inaccurate due to diffusion through the GDL in a realistic PEMFC, the comparison between the water transport rate and the reaction rate can be made reliably. For the anode, the water transport and reaction rate are derived in Eqs. (23) and (24) from the source terms in the mass conservation equation, S_{H_2} and S_{awe}. The water transport rate and the HOR rate are shown in Fig. 12. The molar flux of water was greater than that of hydrogen when α was over 0.5, regardless of the GDLs, stoichiometry, or geometry, as shown in Fig. 12(a) and (b).

$$[H_2]_{oxi} = -\frac{I(x,y)}{2F} \tag{23}$$

$$[H_2O]_{drag} = -\frac{I(x,y)}{F}\alpha(x,y) \tag{24}$$

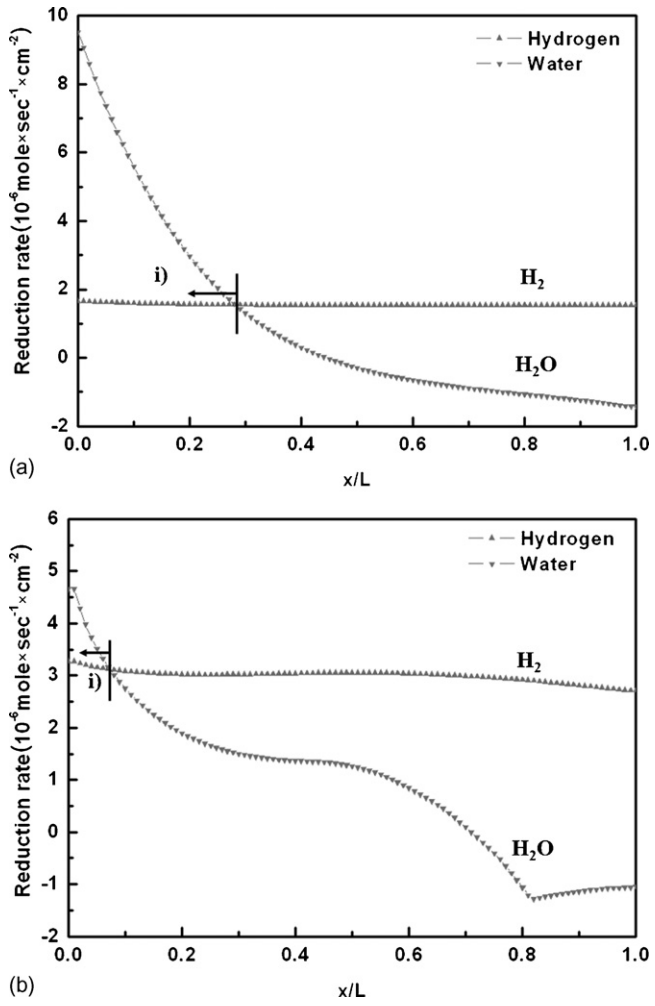

Fig. 12. Hydrogen and water molar flux through the membrane: case 1 (a) and the new grid with GDLs (b).

6. Conclusion

The influence of proton and water transport through PEMFC membranes on the species mole fractions, activation losses, and membrane conductivity was investigated. Criteria for forecasting the species mole fractions in the catalyst layer were validated using CFD analysis when the GDL and BPP ribs were excluded from the computational domain at high stoichiometry. The hydrogen and water mole fractions at the anode had their extrema at $\alpha = 0.5$. The water transport rate was larger than the hydrogen oxidation rate when α was greater than 0.5. Therefore, the membrane conductivity increase when α was below 0.5, and vice versa. The oxygen and water mole fractions at the cathode had their extrema at $\alpha = -0.75$. The oxygen reduction rate was greater than water for $\alpha > -0.75$. Although the oxygen mole fraction had a significant effect on the activation losses, the current density also proved to be a determining parameter. Both the oxygen mole fraction and the current density must be considered to evaluate the activation losses.

The prediction of species mole fractions from alpha criteria was not exact in the computational domain with GDLs at low stoichiometry. When the GDL was sandwiched between the catalyst layer and the bipolar plate, the concentration gradient through the diffusion layer cannot be neglected. That is, the species mole fractions in the catalyst layer were not determined only by proton and water movement through membrane but also by the diffusion rate of hydrogen and oxygen from the GDL. Although the alpha criteria had some errors predicting the maximum and minimum species mole fractions, comparison of the reduction rate of reactants and water on the membrane and the catalyst surfaces was accurately estimated from the alpha criteria.

The diffusion effect in GDLs was not fully investigated in this paper. However, the species mole fractions can be predicted more accurately in the real PEMFC channel by alpha criteria if the diffusion effect in GDLs is complemented. Further study will be needed to define constraints, by applying the alpha criteria for actual conditions and understand the relationship between the species mole fractions and diffusion in the GDL.

Acknowledgement

This work was supported by grant No. R01-2006-000-11298-0 from the Basic Research Program of the Korea Science & Engineering Foundation.

References

[1] R. O'Hayre, S.-W. Cha, W. Colella, F.B. Prinz, Fuel Cell Fundamentals, John Wiley & Sons, New York, 2006.
[2] Kah Wai Lum, James Joseph McGuirk, Journal of The Electrochemical Society 152 (2005) A811–A817.
[3] Dilip Natarajan, Trung Van Nguyen, Journal of The Electrochemical Society 148 (2001) A1324–A1335.
[4] T.E. Springer, M.S. Wilson, S. Gottesfeld, Journal of The Electrochemical Society 140 (1993) 3513–3526.
[5] Sandip Dutta, Sirivatch Shimpalee, J.W. Van Zee, International Journal of Heat and Mass Transfer 44 (2001) 2029–2042.
[6] Paola Costamagna, Chemical Engineering Science 56 (2001) 323–332.
[7] Ugur Pasaogullari, Chao-Yang Wang, Journal of The Electrochemical Society 152 (2005) A380–A390.
[8] Dewan Hasan Ahmed, Hyung Jin Sung, Journal of Power Source 162 (2006) 327–339.
[9] H.-M. Jung, W.-Y. Lee, J.-S. Park, C.-S. Kim, International Journal of Hydrogen Energy 29 (2004) 945–954.
[10] Fang-Bor Weng, Ay Su, Guo-Bin Jung, Yen-Chiao Chiu, Shih-Hung Chan, Journal of Power Source 145 (2005) 546–554.
[11] S. Shimpalee, W.-K. Lee, J.W. Van Zee, H. Naseri-Neshat, Journal of Power Source 156 (2006) 355–368.
[12] S. Shimpalee, W.-K. Lee, J.W. Van Zee, H. Naseri-Neshat, Journal of Power Source 156 (2006) 369–374.
[13] Yun Wang, Chao-Yang Wang, Journal of Power Source 147 (2005) 148–161.
[14] Wang Ying, Tae-Hyun Yang, Won-Yong Lee, J. Ke, Chang-Soo Kim, Journal of Power Source 145 (2005) 572–581.
[15] Wang Ying, Young-Jun Sohn, Won-Yong Lee, J. Ke, Chang-Soo Kim, Journal of Power Source 145 (2005) 563–571.
[16] W.-K. Lee, S. Shimpalee, J.W. Van Zee, Journal of The Electrochemical Society 150 (2003) A341–A348.
[17] T.E. Springer, T.A. Zawodzinski, S. Gottesfeld, Journal of The Electrochemical Society 138 (1991) 2334–2342.
[18] Felix N. Buchi, Gnther G. Scherer, Journal of The Electrochemical Society 148 (2001) A183–A188.
[19] S. Vengatesan, H.-J. Kim, E.A. Cho, S.U. Jeong, H.Y. Ha, I.-H. Oh, S.-A. Hong, T.-H. Lim, Journal of Power Sources 156 (2006) 294–299.
[20] Felix N. Buchi, Supramaniam Srinivasan, Journal of The Electrochemical Society 144 (1997) 2767–2772.
[21] Un Ho Jung, Ki Tae Park, Eun Hee Park, Sung Hyun Kim, Journal of Power Sources 159 (2006) 529–532.
[22] R. Byron Bird, Warren E. Stewart, Edwin N. Lightfoot, Transport Phenomena, 2nd Edition, John Wiley & Sons, Inc., 2007.
[23] S. Shimpalee, J.W. Van Zee, International Journal of Hydrogen Energy 32 (2007) 842–856.